J. Synchrotron Rad. (1998). **5**, 246–251

Application of a Varied-Line-Spacing Grating in a High-Performance Soft X-ray Monochromator

Yonglian Yan,[a]* Eiji Shigemasa[b] and Akira Yagishita[b]

[a]Beijing Synchrotron Radiation Facility, Institute of High Energy Physics, Chinese Academy of Sciences, Beijing 100039, People's Republic of China, and [b]Photon Factory, National Laboratory for High Energy Physics, Oho 1-1, Tsukuba-shi, Ibaraki-ken 305, Japan. E-mail: yanyl@bepc3.ihep.ac.cn

(*Received 4 August 1997; accepted 18 November 1997*)

The design and experimental evaluation of a high-resolution varied-line-spacing-grating monochromator constructed at the Photon Factory are described. Various applications of a varied-line-spacing grating in a high-performance soft X-ray monochromator are discussed.

Keywords: varied-line-spacing gratings; high resolution; aberration; sagittal focusing; self-focusing.

1. Introduction

In the past decades, many types of high-performance soft X-ray monochromators have been developed at synchrotron radiation facilities. The Dragon-type SGM (Chen, 1987; Chen & Sette, 1989) and the SX700-type PGM (Petersen, 1982) are the two types most widely used. Along with the rapid progress of scientific research on soft X-ray spectroscopy, higher and higher resolving powers are required by scientists. With great efforts, a resolving power of ~10000 has been attained with these types of monochromators. People are doing their best to improve them and to develop new configurations for better performances. In doing so, the varied-line-spacing grating (VG) has attracted special attention from beamline designers. In recent years, more and more high-performance varied-line-spacing-grating monochromators (VGM) have been constructed or designed (Koike *et al.*, 1994; Bissen *et al.*, 1995; Reininger & Bissen, 1994; Koike & Namioka, 1995). This demonstrates the belief expressed by McKinney six years ago (McKinney, 1992) that varied-line-spacing gratings will increasingly play a role at synchrotron radiation sources in the future. In this paper, we report the theoretical and experimental evaluation of the varied-line-spacing PGM with a constant included angle (CIA-VPGM) constructed at the Photon Factory in 1996. Two other configurations, *i.e.* the varied-line-spacing SGM (VSGM) and the self-focusing varied-line-spacing PGM (SF-VPGM), are also discussed.

2. Aberrations of a VG

The aberration properties of a VG have been well described by using the light-path function (Noda *et al.*, 1974; Hettrick, 1985; McKinney, 1992). Here we present some basic formulae for the convenience of the following discussion. The optical system is schematically shown in Fig. 1. The light-path function can be expressed as a power series of (w, l),

$$F = F_{00} + wF_{10} + w^2F_{20}/2 + l^2F_{02}/2 + w^3F_{30}/2 + wl^2F_{12}/2 + w^4F_{40}/8 + \ldots \quad (1)$$

The contributions of the individual main aberrations to the resolution can be expressed in terms of the coefficients F_{ij}, which are expressed as

$$F_{ij} = C_{ij} + M_{ij}\, m\lambda/d_0. \quad (2)$$

Here, C_{ij} are the regular coefficients in the light-path function for a constant-line-spacing grating, M_{ij} are the aberration correction coefficients introduced by the line-spacing variation, d_0 is the line spacing at point O, and m and λ are the diffraction order and wavelength, respectively. The line spacing can be described by a power series of w,

$$d(w) = d_0(1 + b_2w + b_3w^2 + b_4w^3 + \ldots), \quad (3)$$

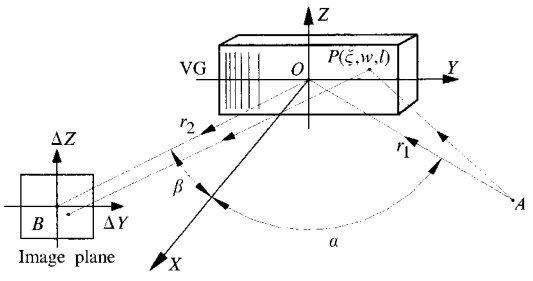

Figure 1
Schematic drawing of the optical path of a diffracted ray. Point O is the centre of the grating. Points A, B and P represent the radiation source, the image and the position where the photon hits the grating, respectively.

Table 1
Results and conditions for the estimation of the resolving power.

Sample	Photon energy (eV)	Grating (lines mm^{-1})	Slit widths, S1/S2 (μm)	Γ_L (meV)	Γ_G (meV)	Resolving power	Expected value
Ar	~244	1000	140/20	113	24.8	~9840	~10000
N_2	~401	1000	70/15	117	40.9	~9800	~10000
Ne	~867	2200	100/15	303	117	~7410	~7500
O_2	~540	2200	100/15				

where b_2, b_3 and b_4 are the first-, second- and third-order correction coefficients of the line-spacing, respectively. With this description, M_{ij} can be expressed with the line-spacing variation coefficients, b_i, as

$$M_{20} = -b_2, \tag{4}$$

$$M_{30} = 2(b_2^2 - b_3)/3, \tag{5}$$

$$M_{40} = -2(b_2^3 - 2b_2b_3 + b_4), \tag{6}$$

$$M_{ij} = 0 \qquad (\text{when } j \neq 0). \tag{7}$$

3. Varied-line-spacing plain-grating monochromator with a constant included angle (CIA-VPGM)

To meet the demands for high-resolution soft X-ray spectroscopy, a high-resolution monochromator was constructed at the Photon Factory in 1996. A detailed description of the design has been given by Yan & Yagashita (1995*b*). The layout and the main parameters are shown in Fig. 2. In this monochromator the focusing mirror M_1 produces a converging beam and a virtual source behind the VPG, and the VPG produces a real image on the exit slit with an imaging distance almost the same as the virtual source distance. With both the included angle and the slits fixed, the focus condition of the grating over the entire energy range can be met quite perfectly. Thus, energy scanning with exact focusing is accomplished by only the rotation of the grating, which is a unique property

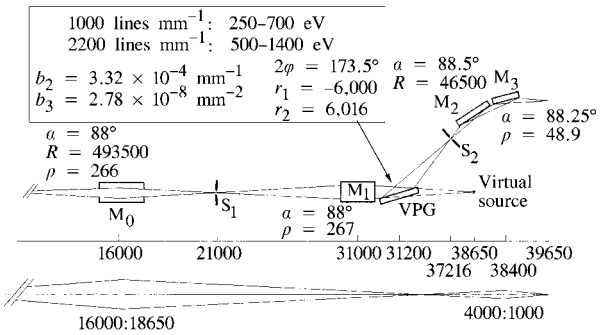

Figure 2
Layout of the CIA-VPGM built at the Photon Factory and its main parameters.

different from those of all other existing monochromators. This type of monochromator is called a CIA-VPGM. It was first developed by Hettrick and his co-workers (Hettrick & Bowyer, 1983; Hettrick & Underwood, 1986; Hettrick *et al.*, 1988) and has been well accepted by many synchrotron radiation beamline designers (Underwood *et al.*, 1996; Koike *et al.*, 1994; Amemiya *et al.*, 1996).

Fig. 3 shows the resolution of this monochromator limited by the slit width, the slope error and the aberrations of the grating, where just the defocus and coma aberrations are shown; the other aberrations are so small that they need not be considered. It is obvious from Fig. 3 that the VPG itself is almost an aberration-free system.

Like the PGM, it is of great importance to have good imaging quality of the focusing mirror between the entrance and exit slits. To conserve the aberration-free property of the VPG, we focused great attention on the design of this mirror. One consideration is to use a demagnification near unity to make its aberration small; in practice, a demagnification of 1.6 is used, which is restricted by the space condition. Another consideration is to set this mirror in a sagittal focusing configuration, which will greatly reduce the aberration due to its figure slope error.

The resolving power has been evaluated from the inner-shell photoabsorption spectra of several gaseous samples: Ne and Ar atoms and N_2 and O_2 molecules. A detailed description of the measurements has been given by

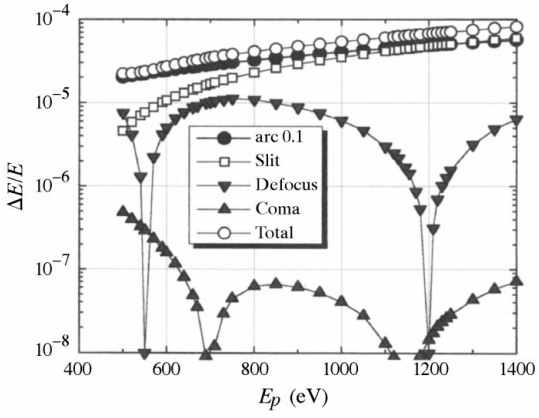

Figure 3
Resolution of the CIA-VPGM (solid circles) and various contributions due to a 20 mm-wide entrance slit and the corresponding width exit slit (open squares), the slope error of 0.1″ of the grating (solid circles), the defocus aberration (down-triangles) and the coma aberration (up-triangles).

Table 2
Parameters of the 24 m HSGM and the VSGMs.

Scheme	$\alpha - \beta$ (°)	D_{PFM}	R_G (mm)	r_1 (mm)	r_2 (mm)	Δr_2 (mm)	Length (mm)	b_2 (mm^{-1})	b_3 (mm^{-2})
1	168.6	10	23832	1700	3246	±220	25846	Constant space	
2	168.6	10	20260	1700	1766	±39	24366	4.374×10^{-4}	-3.205×10^{-7}
3	168.6	5	40520	3400	3532	±78	29732	2.187×10^{-4}	-8.013×10^{-8}

Watanabe *et al.* (1998). Table 1 lists the conditions for the measurements and the results of fitting the spectra with a Voigt function, where Γ_L is the FWHM of the Lorenzian function which arises from the lifetime broadening, and Γ_G is the FWHM of the Gaussian distribution which is used to approximate the transmission function of the monochromator. The resolving power E/Γ_G and the expected values of the resolving power (Yan & Yagishita, 1995*a*) are also listed in Table 1. They agree with each other very well. The spectrum of O_2 shown in Fig. 4 is fairly complicated so that it is difficult to extract the value of the resolving power. However, we can say it is one of the best resolved spectra among those published.

4. Varied-line-spacing spherical-grating monochromator (VSGM)

The application of VSGs in soft monochromators has been discussed by various authors (see, for example, Heidemann & Bittner, 1989; Reininger & Bissen 1994). Here we will provide some discussions from a special viewpoint. Before going ahead, we will give a brief discussion on the principle of designing ultrahigh-resolution-grating monochromators. Among various contributions to the total resolution, those from the slit width and the aberrations of the grating are very closely connected to the configuration of the monochromator; moreover, they are related in some way to the prefocusing system. For a moderate resolving power, *e.g.* several thousands, the aberrations are not a serious problem, but, for an ultrahigh resolving power, they are. One of the key points for designing ultrahigh-resolution monochromators is to reduce the aberrations while conserving the accepting ability. For a definite acceptance angle of the beamline, the defocus, coma and spherical aberrations are proportional to the first, second and third power of the demagnification of the prefocusing system, respectively. By using a smaller demagnification of the prefocusing system and a correspondingly longer entrance arm length of the grating, we can reduce the aberrations of the grating without deteriorating the source size limited resolution and the accepting ability of the grating. This principle is very useful for the design of ultrahigh-resolution-grating monochromators. However, it is not always possible to use a long configuration. Besides space conditions, the properties of the configuration itself impose restrictions. For example, it is difficult to use a long entrance arm length in the SGM, which would lead to a long travelling distance of the exit slit.

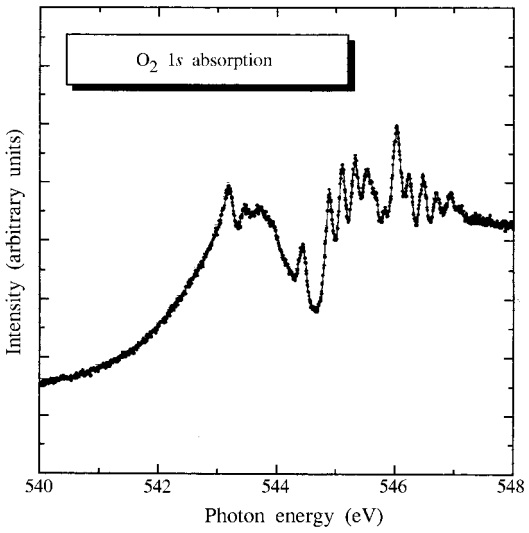

Figure 4
The $1s\sigma \rightarrow$ valence and Rydberg photoabsorption spectrum of the O_2 molecules.

Table 2 lists the main parameters of a standard SGM and two VSGMs. In this table, D_{PFM} is the demagnification of the prefocusing mirror, R_G is the radius of the spherical grating, r_1 is the entrance arm length, and r_2 and Δr_2 are the middle value of the exit arm length and the travelling distance of the exit slit, respectively. The eighth column gives the length of the beamline up to the exit slit, and the last two columns give the line-spacing-variation coefficients of the grating. Scheme 1 is the 24 m high-resolution SGM (24 m HSGM), which was installed at the BL-16 undulator beamline of the Photon Factory in 1995. A resolving power as high as 10000 has been attained using this monochromator (Yagishita *et al.*, 1997). To accept fully the radiation of the undulator, the vertical acceptance angle was adopted to be 0.22 mrad. However, it is impossible to make the coma aberration small enough over the entire energy range with such an acceptance angle, as shown in Fig. 5. In addition, the travelling distance of the exit slit is ±220 mm, which leads to problems with the postfocusing.

The problems mentioned above can be removed by the VSGM. In Scheme 2, D_{PFM} and r_1 are unchanged. Due to the employment of the VSG, the coma aberration vanishes at two energies and is small enough over the entire energy range for a resolving power of 10000. In addition, Δr_2 is only ±39 mm. In this case, we can use the principle discussed above to attain an ultrahigh resolving power. In Scheme 3, D_{PFM} is reduced to half of that for Schemes 1 and 2, while r_1 is doubled. In this

long configuration, Δr_2 becomes ± 78 mm, which is still much shorter than that in Scheme 1. In comparison with Scheme 2, the coma aberration is reduced by a factor of 1/4 as shown in Fig. 5. With Scheme 3, we can obtain a resolving power beyond 20000 with a narrow slit width if we overcome the figure slope error limited resolution of the grating. These three schemes typically embody the roles of the VG.

The design and optimization procedure of the VSGM are described in the following. For a VSGM, the focusing condition is

$$F_{20} = \frac{\cos^2\alpha}{r_1} + \frac{\cos^2\beta}{r_2} - \frac{\cos\alpha + \cos\beta}{R_G} + M_{20}\frac{m\lambda}{d_0} = 0. \quad (8)$$

Expressing r_2 from (8) and substituting it into the expression for F_{30}, we obtain

$$F_{30} = f_{30}(m, d_0, r_1, R_G, a, b, \lambda, M_{20}, M_{30}). \quad (9)$$

The design can be optimized according to the following procedure.

(i) Determine the parameters m, d_0, r_1 and the included angle $\alpha - \beta$ according to the general principles for the design of the SGM.

(ii) Determine M_{20} and M_{30} by imposing $f_{30} = 0$ at two wavelengths λ_1 and λ_2 for a selected value of R_G.

(iii) Calculate r_2 for the entire energy range so that the travelling distance of the exit slit is known.

(iv) Try different values of R_G, repeating steps (ii) and (iii), to make the maximum travelling distance of the exit slit the shortest. Thus, the aberration correction coefficients M_{20} and M_{30} and the radius of the grating R_G are determined. In the above procedure, the two wavelengths can be suitably adjusted to enable the coma aberration to be appropriately distributed over the entire energy range.

(v) Make the spherical aberration vanish at a suitable wavelength to determine the coefficient M_{40}.

Finally, the line-spacing variation coefficients b_2, b_3 and b_4 are calculated from the determined M_{20}, M_{30} and M_{40} according to equations (4)–(7).

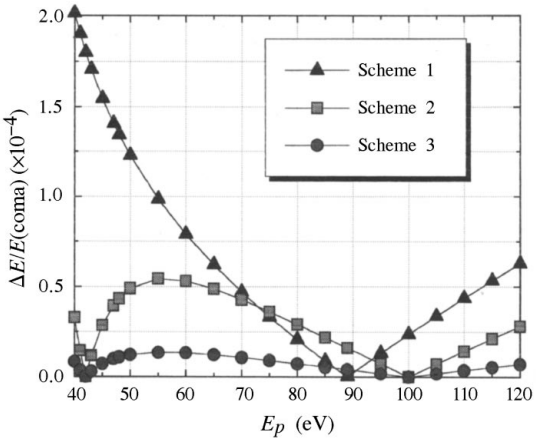

Figure 5
Coma aberration limited resolutions of the 24 m HSGM and the two VSGMs.

5. Self-focusing varied-line-spacing plane-grating monochromator (SF-VPGM)

The SF-VPGM can be regarded as having evolved from the SX700-type PGM. The SX700 is one of the high-performance monochromators known for its wide energy coverage, high resolving power and capability of high-order suppression. However, in the original configuration of the SX700, the performance strongly depends on the focusing quality of an ellipsoidal mirror with high accuracy, which is difficult to manufacture. To overcome this difficulty, many modified configurations have been developed. The best way to overcome this difficulty is perhaps to use a VG to make the virtual image of the grating become a real image with small aberrations. In this case, the focusing mirror is no longer needed and the configuration becomes very simple and clear. Owing to the self-focusing and the aberration-correction capability, the SF-VPGM has very high resolution, while maintaining all the merits of the SX700 mentioned above.

The SF-VPGM was first developed by Harada and co-workers at the Photon Factory in 1989 (Itou *et al.*, 1989). Soon after that, a second one was also built at the Photon Factory (Kakizaki *et al.*, 1992). Up to now, no SF-VPGM with a high resolving power of $\sim$10000 has been reported to our knowledge. In recent years, various VGMs have attracted more and more attention from the beamline designers, while the SF-VPGM seems not to have been paid enough attention. The reason, perhaps, is the complicacy of the scanning mechanism. This problem, according to our analysis, is no more serious for the SF-VPGM than the standard PGM. Using an off-surface rotating mechanism like that used in SX700, the focusing condition can be met quite perfectly over the entire scanning range. A very interesting fact is that the line-spacing variation can partly correct the deviation from the focusing condition due to the imperfection of the scanning mechanism.

As a configuration with variable included angle, both the SX700 and SF-VPGM have good accepting ability, the latter better than the former. Let us investigate the design and optimization procedure of

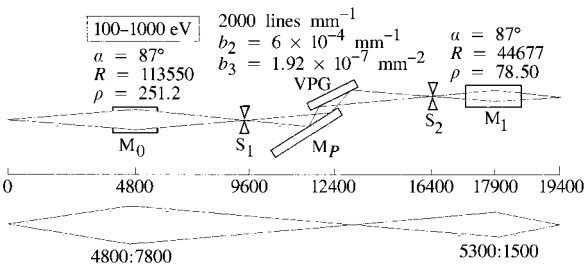

Figure 6
Layout of the SF-VPGM and its main parameters designed for MCD study at the NSRL.

the SF-VPGM. The coefficient F_{20} is expressed as

$$F_{20} = \frac{\cos^2\alpha}{r_1} + \frac{\cos^2\beta}{r_2} - \frac{b^2\lambda}{d_0}. \qquad (10)$$

The parameters r_1 and d_0 can be determined according to some general consideration. We determine the incident angles α at the longest and shortest wavelengths in advance according to the considerations of the reflectivity, dispersion ability and accepting ability of the grating, while the diffraction angles can be calculated using the grating equation. Then we can calculate the values of the parameters r_2 and b_2 by imposing $F_{20} = 0$ at these two wavelengths. Once r_2 and b_2 are determined, the correct values of α and β for energy scanning can be calculated using the equation given by Itou *et al.* (1989). In this procedure, we allow the incident angles at both the shortest and longest wavelengths to have the desired values. This means that we can optimize the SF-VPGM to let its acceptance angle well match the divergency of the source.

The special accepting ability and the high-resolution property of the SF-VPGM make it suitable to various special applications, such as magnetic circular dichroism (MCD) studies. The present MCD beamlines in the world, extracted from bending magnets, accept the radiation above or below the orbital plane by two independent pre-optical systems, as in the double-headed Dragon at the NSLS (Chen, 1992), or by translating and/or rotating some elements of the pre-optical system, as in the SX700/3 at BESSY (Petersen *et al.*, 1993). It is difficult for these complicated systems to obtain the performance expected theoretically. If a monochromator has a large enough vertical acceptance angle over the entire energy range and has high enough resolving power for such a large acceptance angle, the beamline can accept the radiation above or below the orbital plane by simply masking the corresponding radiation.

Following this idea, a SF-VPGM has been designed recently by one of the authors and his colleagues for the bending-magnet MCD beamline at NSRL in Hefei. Fig. 6 shows the schematic layout of this beamline and its main parameters. We use one VPG to convert the energy range from 100 eV to 1000 eV. Both the prefocusing mirror and the postfocusing mirror are bent cylinders, working in a sagittal focusing mode. With such a configuration, the focused spots of the radiation from above and below the orbital plane will have approximately the same location and same shape on the entrance slit, the exit slit and the sample, which is of great importance to MCD studies. Over the entire energy range, the vertical acceptance angle determined by the 170 mm-long grating is about 4.5 times the effective r.m.s. half-angle of the radiation. In this case, we can collect the polarized radiation with a very high figure merit (Chen, 1992). The calculated circular polarization, flux percentage and figure merit are shown in Fig. 7. Fig. 8 shows the contributions to the resolution due to the coma and spherical aberrations. When calculating the aberrations, the full acceptance angle is adopted, which means that the photons extracted from above and below the orbital plane will have, after monochromatization, the same energy within the bandwidth considered. The focusing property, the accepting ability and the resolving power of this design have been confirmed by ray-tracing simulations.

6. Summary

In this paper, three VGMs are discussed. Each of them can be a candidate for the design of ultrahigh-resolution soft X-ray monochromators. The CIA-VPGM and the VSGM have similar characteristics.

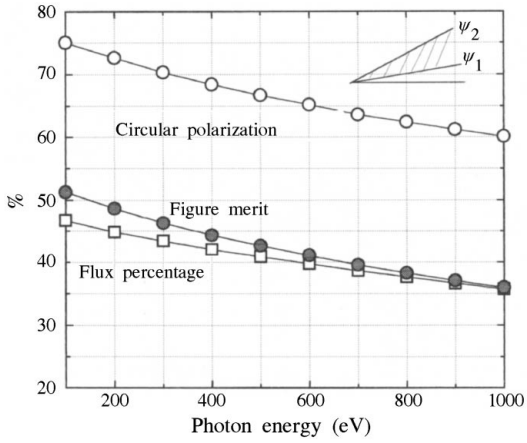

Figure 7
The calculated circular polarization, flux percentage and figure merit of the SF-VPGM for MCD study. The outer edge of the aperture is determined by the acceptance angle of the grating, and the inner edge is set to be 0.1 mrad.

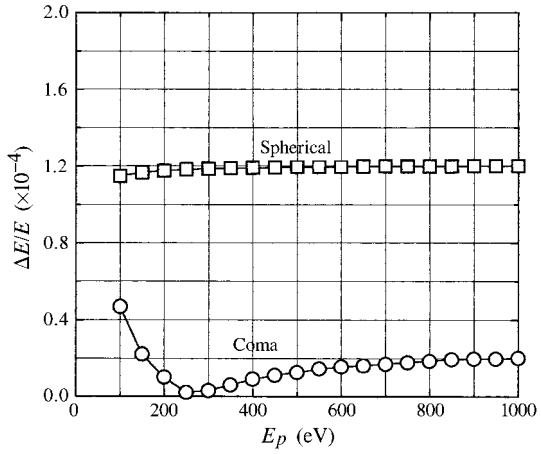

Figure 8
Aberration-limited resolution of the SF-VPGM for MCD study. When calculating the aberrations, the full accepting angles are included.

The CIA-VPGM gives a fine image at the sample position over the entire energy range. However, the addition of a focusing mirror between the entrance and exit slit will lead to problems with the alignment and, needless to say, will reduce the throughput. The VSGM can make the travelling distance of the exit slit much shorter than the SGM. Therefore, if fine focusing at the sample position is not strongly required, the VSGM can be regarded as a good choice. As a configuration with variable included angle, the SF-VPGM has some unique advantages in comparison with the other two configurations, which make it very good for some special applications.

The performance of the VGM depends extremely on the quality of the VG. In recent years, the so-called second-generation holographic grating has been developed and is commercially available, which is generated by the interference of two aspherical wavefronts and can be accurately made to have the required line-spacing variation (Palmer, 1989). The successes of some designs mentioned in this paper imply that the manufacturing technology of the VG has been developed to a very high level so that designers of synchrotron radiation beamlines can be assured of using it in their designs.

The authors thank Professor T. Matsushita for his support and continuous encouragement. We also thank Professor T. Miyahara for his helpful discussions concerning this work. One of the authors (YY) thanks the Ministry of Education, Science and Culture of Japan for funding. The main parts of this work were carried out during a period when he stayed at the Photon Factory as a visiting scientist under this support. He also thanks his collaborators at BSRF for their collaboration on designing the monochromator for the MCD study mentioned in this paper.

References

Amemiya, K., Kitajima, Y., Ohta, T. & Ito, K. (1996). *J. Synchrotron Rad.* **3**, 282–288.
Bissen, M., Fisher, M., Rogers, G., Eisert, D., Kleman, K., Nelson, T., Mason, B., Middleton, F. & Höhest, H. (1995). *Rev. Sci. Instrum.* **66**(2), 2072–2074.
Chen, C. T. (1987). *Nucl. Instrum. Methods*, A**256**, 595–604.
Chen, C. T. (1992). *Rev. Sci. Instrum.* **63**(1), 1229–1233.
Chen, C. T. & Sette, F. (1989). *Rev. Sci. Instrum.* **60**, 1616–1621.
Heidemann, K. F. & Bittner, R. F. (1989). *SPIE*, **1140**, 508–517.
Hettrick, M. C. (1985). *Appl. Opt.* **24**, 1737.
Hettrick, M. C. & Bowyer, S. (1983). *Appl. Opt.* **22**, 3921–3924.
Hettrick, M. C. & Underwood, J. H. (1986). *AIP Conf. Proc.* **147**, 237–245.
Hettrick, M. C., Underwood, J. H., Batson, P. J. & Eckart, M. J. (1988). *Appl. Opt.* **27**, 200–202.
Itou, M., Harada, M. I. & Kita, T. (1989). *Appl. Opt.* **28**, 146–151.
Kakizaki, A., Kinoshita, T., Harasawa, A., Ohkuma, H., Ishii, T., Taniguchi, M., Ikezawa, M., Soda, K. & Suzuki, S. (1992). *Nucl. Instrum. Methods*, A**311**, 620–627.
Koike, M., Beguiristain, R., Underwood, J. H. & Namioka, T. (1994). *Nucl. Instrum. Methods*, A**347**, 273–277.
Koike, M. & Namioka, T. (1995). *Rev. Sci. Instrum.* **66**(2), 2144–2146.
McKinney, W. R. (1992). *Rev. Sci. Instrum.* **63**(1), 1410–1414.
Noda, H., Nomioka, T. & Seya, M. J. (1974). *Opt. Soc. Am.* **64**, 1037.
Palmer, C. (1989). *J. Opt. Soc. Am.* A**6**, 1175–1188.
Petersen, H. (1982). *Opt. Commun.* **40**, 402–407.
Petersen, H., Willmann, M., Schäfers, F. & Gudat, W. (1993). *Nucl. Instrum. Methods*, A**333**, 594–598.
Reininger, R. & Bissen, M. (1994). *Nucl. Instrum. Methods*, A**347**, 269–272.
Underwood, J. H., Gullikson, E. M., Koike, M., Batson, P. C., Denham, P. E., Steele, R. & Tackaberry, R. (1996). *Rev. Sci. Instrum.* **67**(9), 1–5.
Watanabe, M., Toyoshima, A., Azuma, Y., Hayaishi, T., Yan, Y. & Yagishita, A. (1998). *SRI'97 Meeting*. Abstract 7PA13.
Yagishita, A., Shigemasa, E. & Yan, Y. (1997). *J. Phys. IV*, **7**(C2), 287–295.
Yan, Y. & Yagishita, A. (1995*a*). KEK Report 95–9. KEK, Tsukuba, Ibaraki 305, Japan.
Yan, Y. & Yagishita, A. (1995*b*). *Proceedings of the Fourth International Conference on Synchrotron Radiation Source & Second Asian Forum on Synchrotron Radiation*, Kyongju, Korea, 25–27 October, pp. 615–621. Pohang Accelerator Laboratory, POSTECH, Pohang, Kyuag Buk, Korea.